Seasonally different carbon flux changes in the Southern Ocean in response to the southern annular mode

J. Hauck,[1] C. Völker,[1] T. Wang,[1] M. Hoppema,[1] M. Losch,[1] and D. A. Wolf-Gladrow[1]

Received 22 March 2013; revised 30 October 2013; accepted 10 November 2013.

[1] Stratospheric ozone depletion and emission of greenhouse gases lead to a trend of the southern annular mode (SAM) toward its high-index polarity. The positive phase of the SAM is characterized by stronger than usual westerly winds that induce changes in the physical carbon transport. Changes in the natural carbon budget of the upper 100 m of the Southern Ocean in response to a positive SAM phase are explored with a coupled ecosystem-general circulation model and regression analysis. Previously overlooked processes that are important for the upper ocean carbon budget during a positive SAM period are identified, namely, export production and downward transport of carbon north of the polar front (PF) as large as the upwelling in the south. The limiting micronutrient iron is brought into the surface layer by upwelling and stimulates phytoplankton growth and export production but only in summer. This leads to a drawdown of carbon and less summertime outgassing (or more uptake) of natural CO_2. In winter, biological mechanisms are inactive, and the surface ocean equilibrates with the atmosphere by releasing CO_2. In the annual mean, the upper ocean region south of the PF loses more carbon by additional export production than by the release of CO_2 into the atmosphere, highlighting the role of the biological carbon pump in response to a positive SAM event.

Citation: Hauck, J., C. Völker, T. Wang, M. Hoppema, M. Losch, and D. A. Wolf-Gladrow (2013), Seasonally different carbon flux changes in the Southern Ocean in response to the southern annular mode, *Global Biogeochem. Cycles*, *27*, doi:10.1002/2013GB004600.

1. Introduction

[2] The subpolar and polar Southern Ocean is a large-scale upwelling region where carbon- and nutrient-rich water masses are brought to the surface. In preindustrial times, this led to net outgassing of CO_2 into the atmosphere [*Hoppema*, 2004; *Mikaloff Fletcher et al.*, 2007]. Since then, the atmospheric CO_2 concentration has been rising due to anthropogenic CO_2 emissions such that the same amount of upwelling does not lead to net CO_2 outgassing anymore. Today, the Southern Ocean is a net sink for CO_2 and one of the main gateways for anthropogenic CO_2 into the ocean's interior [*Khatiwala et al.*, 2009]. It plays a pivotal role in the marine and global carbon cycle by defining the nutrient concentration in the global thermocline and by regulating atmospheric CO_2 concentrations [e.g., *Marinov et al.*, 2006]. Recently, it was emphasized how the upwelling in the Southern Ocean closes the meridional overturning circulation, and its significance for the transport of heat, fresh water, and carbon was highlighted [*Marshall and Speer*, 2012].

[3] One single annular pattern dominates the internal atmospheric variability in the Southern Hemisphere; the so-called southern annular mode (SAM) is characterized by a SAM index that can be calculated as the leading empirical orthogonal function (EOF) of sea level pressure or geopotential height fields [*Thompson and Wallace*, 2000]. A positive SAM index indicates a stronger than usual pressure gradient between the high-latitude low and the midlatitude high regimes. In such a case, the jet stream is displaced poleward, and westerly winds become stronger south of about 45°S [*Hall and Visbeck*, 2002; *Thompson and Wallace*, 2000]. In recent decades, there was a positive trend in the SAM index, that is a shift toward its positive phase [*Marshall*, 2003], driven by the loss of stratospheric ozone ("ozone hole") and the increase in greenhouse gas concentrations [*Thompson et al.*, 2011]. The trend toward the high-index polarity of the SAM is most pronounced in summer and is predicted to continue in the future [*Marshall*, 2003; *Thompson et al.*, 2011].

[4] The ocean's response to the SAM trend is under debate. Coarse-resolution and eddy-permitting models agree with observations that the initial response of the ocean is a stronger northward Ekman transport and a southward shift of the Antarctic Circumpolar Current (ACC) by 50 to 80 km on average [e.g., *Böning et al.*, 2008; *Hall and Visbeck*, 2002;

Additional supporting information may be found in the online version of this article.

[1]Alfred Wegener Institute, Helmholtz Centre for Polar and Marine Research, Bremerhaven, Germany.

Corresponding author: J. Hauck, Alfred Wegener Institute, Helmholtz Centre for Polar and Marine Research, Postfach 12 01 61, 27515 Bremerhaven, Germany. (judith.hauck@awi.de)

0886-6236/13/10.1002/2013GB004600

Sen Gupta and England, 2006; *Hallberg and Gnanadesikan*, 2006; *Hogg et al.*, 2008; *Screen et al.*, 2009; *Spence et al.*, 2010]. While this is all of the response in coarse-resolution models, eddy-permitting models and observations additionally reveal an increased eddy activity with a lag of 2 to 3 years [*Meredith and Hogg*, 2006; *Screen et al.*, 2009]. The southward eddy fluxes are thought to partly compensate for the changes in the wind-driven circulation [e.g., *Hallberg and Gnanadesikan*, 2006; *Hogg et al.*, 2008; *Screen et al.*, 2009; *Böning et al.*, 2008; *Marshall and Speer*, 2012]. In recent eddy-permitting and eddy-resolving models, however, a doubling of the wind stress increased the overturning by 70% with nearly unaltered ACC transport [*Meredith et al.*, 2012; *Morrison and Hogg*, 2013] (see also *Dufour et al.* [2012]).

[5] The interannual variation in Southern Ocean circulation patterns causes variability in biogeochemical cycles [*Lovenduski and Gruber*, 2005; *Lenton and Matear*, 2007; *Lovenduski et al.*, 2007]. *Lenton and Matear* [2007, hereafter referred to as LM07] and *Lovenduski et al.*[2007, hereafter referred to as Lov07] hypothesized that a significant decrease of the Southern Ocean CO_2 sink efficiency is associated with the ongoing trend to a more positive SAM.

[6] *Le Quéré et al.* [2007] suggested that the Southern Ocean CO_2 sink had weakened relative to the trend in atmospheric CO_2 concentrations already in the 1990s [see also *Zickfeld et al.*, 2008; *Law et al.*, 2008; *Le Quéré et al.*, 2008, for further discussion]. The reduction in CO_2 uptake relative to the atmospheric CO_2 increase was related to the strengthening of subpolar westerlies and consecutive upwelling of carbon-rich deep water during the positive phase of the SAM. But increased winds might as well strengthen the Southern Ocean sink in the future once the partial pressure of CO_2 in the surface layer exceeds that of the deep ocean [*Zickfeld et al.*, 2008; *Matear and Lenton*, 2008].

[7] Previous studies analyzed different aspects of the CO_2 flux variability in response to the SAM trend [Lov07, LM07, *Lovenduski et al.*, 2008], but the complete set of all physical and biological changes in the perturbed upper ocean carbon budget has not been quantified until very recently [*Dufour et al.*, 2013, hereafter referred to as D13]. None of the studies investigated the seasonality of the response to the SAM despite the SAM's pronounced seasonality [*Marshall*, 2003; *Thompson et al.*, 2011] nor the succession of physical to chemical and biological changes. Questions to be answered include the following: How much carbon does stronger upwelling bring into the surface layer and what is its fate? Is the response the same throughout all seasons? How do phytoplankton functional types react and how does biological productivity contribute to the carbon budget at a positive SAM event?

[8] The hypothesis of Lov07 that primary production does not contribute significantly to the variability of CO_2 fluxes was recently challenged by *Wang and Moore* [2012], but they focused on general statements about long-term trends in the last decades and did not analyze their hindcast simulation with respect to positive SAM events. Here we attempt to unravel the relative roles of circulation, phytoplankton functional types, and total productivity on controlling CO_2 sea-air exchange variability during a positive SAM event. Our model differs from coarse-resolution models that were previously used to study changing carbon fluxes in the Southern Ocean (Lov07, LM07), as we succeed in modeling silicate limitation in the Southern Ocean, use an active sea-ice model, consider variable phytoplankton stoichiometry, and use a higher resolution (see section 2).

[9] This study aims to contribute to the understanding of the variability of Southern Ocean CO_2 fluxes and the role of biology and to present a seasonally resolved budget for the SAM-perturbed upper ocean carbon cycle. We present our model setup in section 2 and investigate the interannual variability of the system, driven by variations in the SAM index, and present a full carbon budget for the system perturbed by a positive SAM event in section 3. We consider the system's response to a positive SAM event with lags of 0 to 12 months and the different responses during different seasons in section 4 and conclude in section 5.

2. Model

[10] We use the Massachusetts Institute of Technology general circulation model (MITgcm) [*Marshall et al.*, 1997; *MITgcm Group*, 2012]. We use a nearly global model configuration without the Arctic Ocean, on a $2^\circ \times 0.38$ to 2° grid. In the Southern Hemisphere, the latitudinal spacing is 2° times the cosine of the latitude to better resolve the region of interest, namely, the Southern Ocean. In addition, we increase the resolution to about half a degree around the equator to resolve the equatorial undercurrent [*Aumont et al.*, 1999]. The thickness of the 30 vertical layers increases from 10 m at the surface to 500 m below a depth of 3700 m, and the bathymetry product of *Timmermann et al.* [2010] is used. A thermodynamic and dynamic sea-ice model [*Losch et al.*, 2010] is coupled to the ocean model. Parameterizations of effects of mesoscale eddies [*Gent and McWilliams*, 1990] and density-driven down-sloping flows on continental shelves [*Campin and Goosse*, 1999] are applied.

[11] We use the ecosystem and biogeochemistry model REcoM-2 (Regulated Ecosystem Model, version 2; see supporting information for a detailed model description and equations). REcoM-2 is based on the *Geider et al.* [1998] model that allows phytoplankton to adapt their stoichiometry to light and temperature conditions and to nutrient supply. Consequently, the ratios of C:N and C:Chl vary in response to different growth conditions. An earlier version of the model (REcoM), with one phytoplankton class, was developed by *Schartau et al.* [2007] and extended by *Hohn* [2009]. REcoM-2 represents two phytoplankton functional types, namely, diatoms and nanophytoplankton. Calcium carbonate production is computed as a function of the gross nanophytoplankton production. The model carries eight phytoplankton tracers (carbon, nitrogen, chlorophyll, calcium carbonate, and silicate pools). Further tracers are dissolved nutrients (nitrate DIN, silicate DSi, and iron DFe), DIC and total alkalinity (ALK), detritus with pools of nitrogen, carbon, silicate, iron, and calcium carbonate, one type of zooplankton with carbon and nitrogen reservoirs, and dissolved organic nitrogen and carbon. Grazing is implemented as a sigmoidal function of prey density [*Gentleman et al.*, 2003]. The sinking speed for detritus increases vertically [*Kriest and Oschlies*, 2008]. REcoM-2 allows for accumulation of sinking material in one single sediment layer. Carbon chemistry and CO_2 fluxes follow

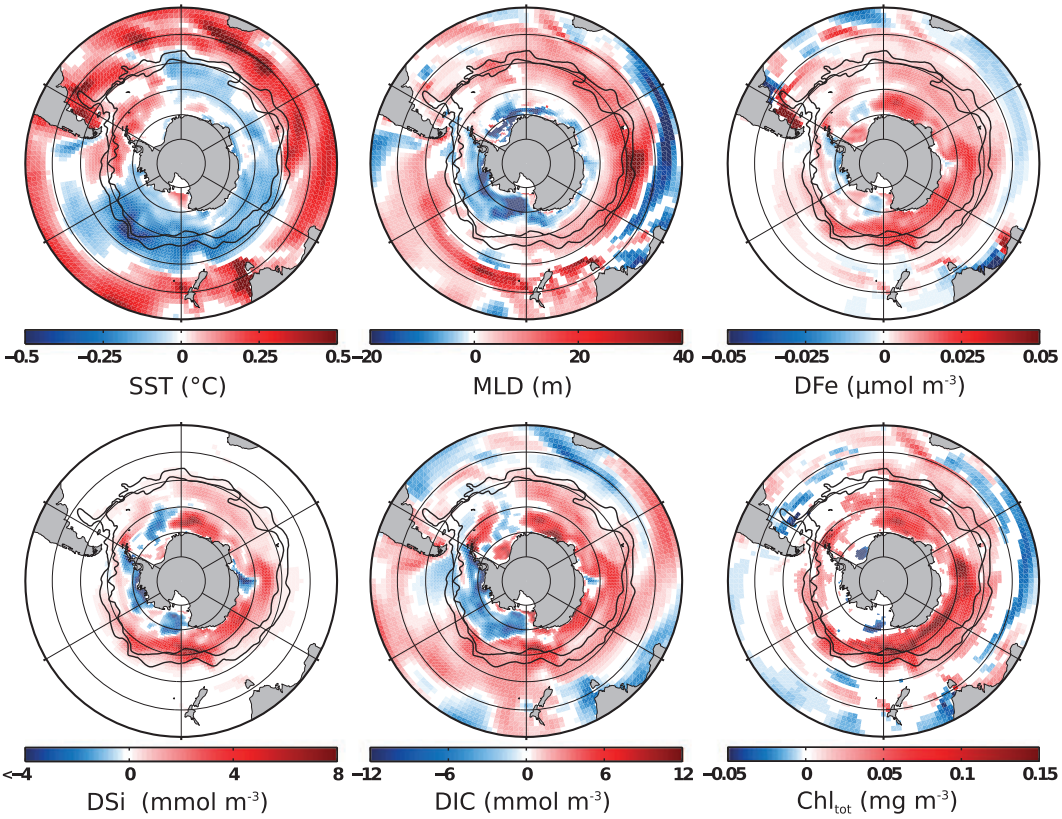

Figure 1. Regression coefficients of state variables regressed onto the SAM index. All numbers are per one unit increase in the standardized SAM index. Shown are regressions onto the SAM index of sea surface temperature (SST, 0–10 m, 0 lag), mixed layer depth (MLD, 0 lag), dissolved iron (DFe, 0–10 m, 4 months lag), dissolved silicate (DSi, 0–10 m, 4 months lag), dissolved inorganic carbon (DIC, 0–10 m, 4 months lag), and total chlorophyll (Chl_{tot}, 0-10 m, 4 months lag). White areas indicate no trend or no significant correlation at the 95% confidence level. Black lines show, from north to south, subantarctic front and polar front from *Orsi et al.* [1995].

the Ocean Carbon Model Intercomparison Project protocols (http://www.ipsl.jussieu.fr/OCMIP/), and a weak alkalinity restoring is applied (see supporting information). Gas exchange is parameterized using the *Wanninkhof* [1992] formulation considering chemical enhancement. The effective gas exchange is proportional to the ice-free area in each grid box.

[12] Our model has several advantages compared to previous coarse-resolution models of the Southern Ocean carbon cycle (Lov07, LM07). In contrast to LM07, we can now estimate biogeochemical export based on prognostically modelled different phytoplankton and zooplankton types. We explicitly simulate nanophytoplankton, calcifiers (as part of the nanophytoplankton), and diatoms as Lov07, but we do not include diazotrophs, as they were shown to be negligible components in the Southern Ocean [*Moore et al.*, 2004]. Both our model and that of Lov07 explicitly resolve the iron cycle. In contrast to LM07 and Lov07, our model includes a dynamic and thermodynamic sea-ice module. We use the same forcing, but our spatial model resolution is approximately a factor of two higher than in Lov07's study. We succeed in modeling silicate limitation between 30°S and 60°S (see Figure S3) in contrast to Lov07 (as reported in the model evaluation by *Moore et al.* [2004] that Lov07 refer to), and we allow for adaptation of intracellular stoichiometry in phytoplankton in response to environmental conditions. The variable C:Chl ratio is important when addressing whether the apparent increase of chlorophyll in satellite observations [*Lovenduski and Gruber*, 2005] can be explained by additional iron input that induce changes in the C:Chl ratio [*Lenton et al.*, 2009] or alternatively by actually increased carbon biomass.

[13] The model is spun-up from 1900 to 1947, and the period from 1948 to 2010 is simulated with 6-hourly interannually varying forcing (NCEP/NCAR-R1) and is used for the analysis. Constant atmospheric CO_2 of 278 ppm is prescribed, and therefore, we refer to "natural" CO_2 fluxes. Initialization and forcing fields and an evaluation of the mean state and seasonal cycle are detailed in the supporting information.

3. Interannual Variability

[14] We investigate the influence of the SAM on the interannual variability of the Southern Ocean (south of 30°S) physics, ecosystem and carbon fluxes, and the succession of the perturbations to gain insights into the mechanisms responsible for ecosystem and carbon flux variability. For this purpose, we regress monthly deseasonalized anomalies of state variables and carbon fluxes at each model grid

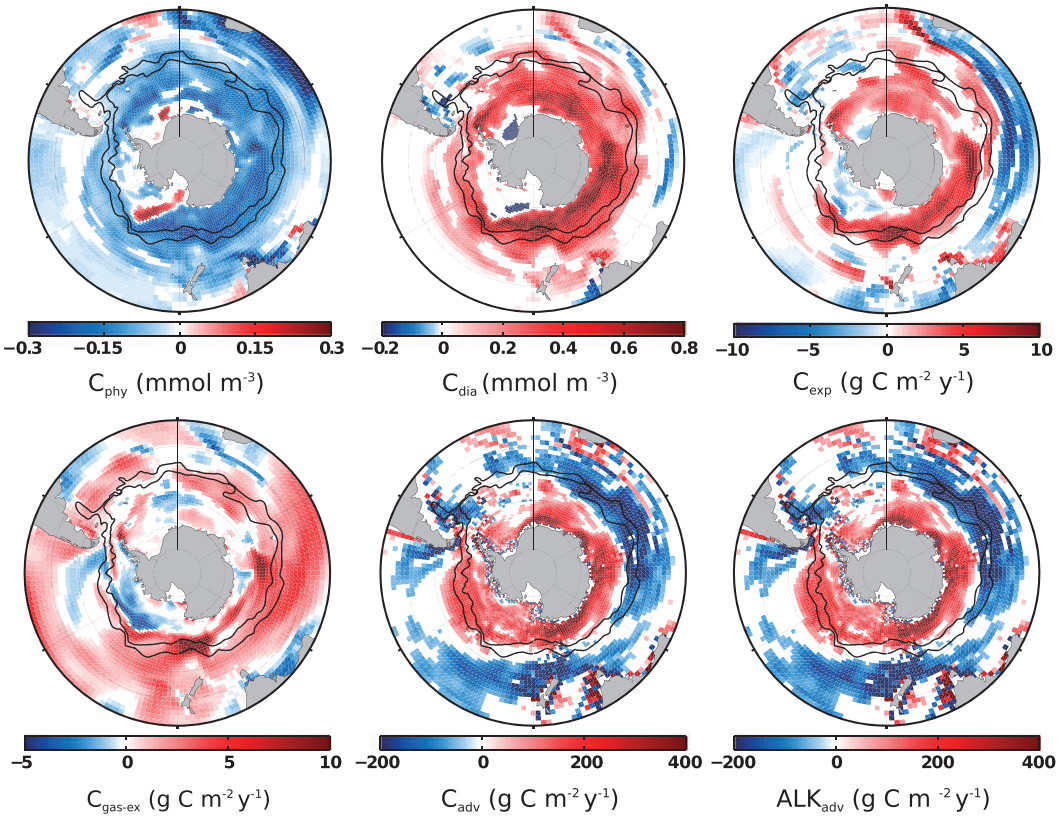

Figure 2. Same as Figure 1. Shown are regressions onto the SAM index all with a 4 months lag of small phytoplankton carbon (C_{phy}, 0–10 m), diatom carbon (C_{dia}, 0–10 m), POC export at 100 m (C_{exp}), sea-air CO_2 flux ($C_{gas\text{-}ex}$), upward advection of DIC at 100 m (C_{adv}), and upward advection of alkalinity at 100 m (Alk_{adv}).

point to the monthly SAM index considering a lag of 0 to 12 months. The monthly time series of the SAM index is shifted by 0 to 12 months and leads the monthly ocean variable time series. We refer to the *annual mean response* when the entire time series is considered, to the *summer response* when only the ocean variables of the months December to February are used for the regression (still considering the leading SAM index with 0 to 12 months lag), and we refer to the *winter response* when the ocean variables from June to August are regressed onto the SAM index with a lag time of 0 to 12 months.

[15] Anticipating the outcome of our analyses, results will be presented at the approximate time of maximum response, i.e., with 0 lag for physics and with a lag of 4 months for nutrients, primary production, and carbon fluxes, before the time series with all possible lags, as well as different seasons will be analyzed. We use the SAM index from 1948 to 2010 based on the leading EOF of sea level pressure anomalies south of 20°S from the NCEP-NCAR Reanalysis (http://jisao.washington.edu/data/aao/slp). The SAM index is standardised to the period 1979 to 2010 with a mean of zero and a standard deviation of one. We apply a running 8 month mean filter to smooth the SAM index (see supporting information).

3.1. Response of Southern Ocean Physics to SAM

[16] The patterns in sea surface temperature (SST) variability, as depicted by a regression of SST onto the SAM index (Figure 1), agree with satellite-based observations [*Lovenduski and Gruber*, 2005; *Thompson et al.*, 2011]. Regions of decreasing temperature are found in the Antarctic and polar frontal zones in the Pacific and Indian Ocean sectors and extend to the subtropical zone in the Pacific. In contrast, temperature increases around the Antarctic Peninsula, in parts of the Ross, Weddell, and Prydz Bay Gyres and in the entire subtropical zone with the single exception of a cold tongue in the Pacific. While the general pattern is in line with observations [*Lovenduski and Gruber*, 2005; *Thompson et al.*, 2011], the warming north of 50°S to 60°S seems to be too zonal in our model and might be overestimated.

[17] The mixed layer depth (MLD), calculated using a density criterion [*Kara et al.*, 2000], deepens in a broad band around the polar front (PF) and shoals along the Antarctic coast with increasing SAM index (shown for lag 0 in Figure 1). An exception is the east Pacific sector, where the MLD becomes shallower from the Antarctic continent up to the subantarctic front. The general pattern of MLD variability is consistent with the inference of increased mixed layer depths north of the PF by *Lovenduski and Gruber* [2005]. The boundary line between shoaling and deepening, however, appears much further south in the Atlantic and Indian basins in our model. The response of MLD to the SAM is more zonally uniform in our model than in the data-based estimate of *Sallée et al.* [2010] and very similar to other models' responses (D13).

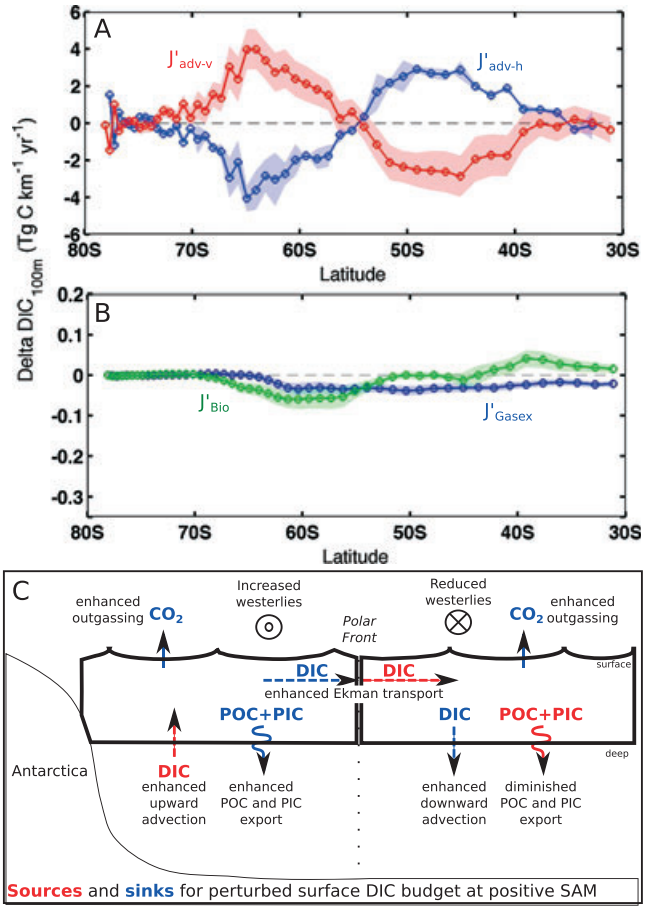

Figure 3. Annual mean perturbation of natural carbon fluxes in the upper Southern Ocean (100 m) per one unit increase in the standardized SAM index. The 2-D fields are integrated zonally and reported per kilometer in meridional direction. Negative fluxes indicate a sink for the perturbed surface DIC inventory (more export production or more CO_2 release into the atmosphere). The shaded areas show the 95% confidence intervals. (a) Contribution of vertical advection (J'_{adv-v}) and of divergence of horizontal advection (J'_{adv-h}). (b) Contribution of export production (J'_{Bio}, green) and sea-air CO_2 exchange (J'_{Gasex}, blue). (c) Idealized sketch of the perturbed carbon fluxes (red = source, blue = sink for surface DIC inventory). Dashed arrows indicate advection anomalies, solid arrows gas-exchange, and wiggled arrows export production. See Table 1 for the magnitude of the fluxes and the differences between summer and winter.

[18] Changes in upwelling and northward Ekman transport will be discussed in the context of carbon transport in section 3.3.

3.2. Response of Nutrients and Biological Production to SAM

[19] The response of surface silicate (Figure 1) to a positive SAM event is restricted to the Southern Ocean south of the PF. The additional silicate seems to be used up before it can be advected further north, as significant regression coefficients for vertical advection of silicate at 100 m, and surface silicate concentration with the SAM index only appear south of the PF (not shown). The change of silicate concentration in response to the SAM ranges from –7.4 mmol m^{-3} to +8.0 mmol m^{-3}; on average, silicate increases by 0.8 mmol m^{-3} south of 50°S. The surface iron concentration increases south of the subantarctic front (SAF), except for small areas in the central Ross and Weddell Gyres and in the coastal western Antarctic Peninsula region (Figure 1). North of the SAF, iron increases between 40°S and 50°S in the Atlantic and Indian Ocean sectors. On average, iron increases by 0.008 μmol m^{-3} south of 50°S.

[20] We see a general decrease of nanophytoplankton carbon biomass during positive SAM (Figure 2). Diatoms thrive everywhere in and south of the ACC except in parts of the Ross and Weddell Gyres (Figure 2). As diatoms dominate the phytoplankton assemblage, this leads to an overall increase of total chlorophyll; chlorophyll anomalies are positively correlated with SAM anomalies south of 50°S and are in sum not significantly different from 0 north of 50°S. The regression of satellite-based chlorophyll data to SAM led *Lovenduski and Gruber* [2005] to suggest that an increase of chlorophyll south of the PF is induced by increased iron supply from below, whereas the reduction of chlorophyll north of the PF is caused by an increased mixed layer depth. We find a similar correlation pattern of chlorophyll, but the areas of iron increase and MLD deepening overlap in our model: the mixed layer is not only deeper north of the PF but also between approximately 60°S and 40°S in the Atlantic, Indian, and west Pacific sectors and north of 60°S in the east Pacific sector. We suggest that the additional iron is responsible for the chlorophyll increase in the south where iron limitation controls diatom growth (Figure S3) and that the combined factors of persistent silicate limitation, deeper mixed layer, and little additional iron are likely responsible for the observed stagnancy and local reduction of total carbon biomass and chlorophyll north of the PF (Figure 2).

[21] In high-nutrient low-chlorophyll regions, such as the Southern Ocean south of the PF, large diatoms can increase their biomass when iron becomes available [*de Baar et al.*, 2008], probably by a combination of increased diatom growth rate and increased grazing pressure on small phytoplankton. In the simulation, this response is caused by higher growth rates when iron limitation is reduced.

3.3. Response of Carbon Inventory and Fluxes

[22] In response to positive SAM phases, we find the same positive anomalies of vertical DIC transport by (more upward) advection at 100 m south of 55°S that were previously suggested [Lov07, LM07, *Le Quéré et al.*, 2007]. In contrast, D13 found that vertical diffusion is the most important processes of carbon transport across the base of the mixed layer during positive SAM phases and that vertical advection may play an important role only in bringing carbon to the base of the mixed layer. We do not discriminate between vertical advection to and across the base of the mixed layer so that our findings are congruent with D13.

[23] In addition, we find negative anomalies of carbon transport (more downward advection) north of 55°S (Figure 2) that have not been reported before because carbon transport was not available directly [Lov07, LM07, *Le Quéré et al.*, 2007]. D13 report more isoneutral diffusive

Table 1. Seasonally Resolved Natural Carbon Flux Anomalies (Pg C yr^{-1} Per Unit Standardized SAM index) for the Upper 100 m[a]

	Annual Average	Summer	Winter
south of 55°S			
Upward advection J'_{adv-v}	3.6 ± 1.9	3.9 ± 2.5	3.1 ± 2.6
POC and PIC export J'_{Bio}	0.08 ± 0.04	0.19 ± 0.10	0.007 ± 0.005
CO_2 flux J'_{Gasex}	0.04 ± 0.02	-0.09 ± 0.03	0.10 ± 0.04
across 55°S			
horizontal advection $\int J'_{adv-h} dy$	3.6 ± 1.2	3.6 ± 1.9	3.3 ± 1.8
north of 55°S			
Upward advection J'_{adv-v}	-3.4 ± 2.5	-4.1 ± 3.6	-2.9 ± 3.3
POC and PIC export J'_{Bio}	-0.03 ± 0.05	0.20 ± 0.09	-0.08 ± 0.06
CO_2 flux J'_{Gasex}	0.09 ± 0.03	-0.01 ± 0.05	0.13 ± 0.06

[a]Positive CO_2 flux anomaly indicates additional outgassing or less uptake. Note that the horizontal advection across 55°S is the integral of the flux divergence J'_{adv-h} between the southern boundary and 55°S.

carbon transport out of the mixed layer, supporting that a downward transport occurs.

[24] The stronger upwelling (and presumably entrainment) of deep water increases nutrient concentrations and causes elevated diatom and total phytoplankton production south of the PF. As a result, more particulate organic carbon sinks out of the surface layer (Figure 2).

3.3.1. The SAM-Perturbed Surface 100 m Carbon Budget

[25] The effects of the individual carbon fluxes on the DIC budget in the upper 100 m are calculated following the equations given in Lov07. The monthly model output (monthly means) from 1949 to 2010 is used for the following offline calculation. The terms J'_{Gasex}, J'_{Bio}, J'_{adv-v}, and J'_{adv-h} all describe carbon flux anomalies as regressed onto the SAM index with a four months lag and integrated over the 100 m surface layer. J'_{Bio} accounts for anomalies with respect to the export flux of particulate organic and inorganic carbon across the 100 m horizon. J'_{Gasex} denotes changes in gas exchange, and J'_{adv-v} denotes changes in the vertical advection of DIC across the 100 m horizon. J'_{adv-h} is defined as the divergence of horizontal (northward) DIC advection anomalies in the 100 m surface layer. The contributions of vertical and horizontal diffusion were calculated but were found to be insignificant. They are likely to play a role across the base of the mixed layer [D13], but this is not resolved by our analysis. The only differences to Lov07 are that we integrate over the top 100 m and not over the mixed layer depth and that we use vertical and horizontal (northward) advection of DIC that are calculated either online (vertical advection) or offline (northward advection, as the product of northward velocity and DIC concentration). In contrast to Lov07, we calculate the changes in physical carbon transport directly and do not infer circulation changes from the balance between changes in surface DIC, J'_{Gasex}, and J'_{Bio}. It should be noted that the advective and diffusive fluxes that we present also contain fluxes from parameterization of the advective and diffusive effect of eddies. Their contribution, however, is likely to be low, as we are using the tapering scheme by *Large et al.* [1997], which effectively switches off the parameterization near the surface. This is unlike *Lovenduski et al.* [2013], who found that the parameterized eddy fluxes counteract the Eulerian mean advection to some degree.

[26] The results are presented in Figures 3a and 3b as the zonal and vertical integrals of the anomalies regressed to the SAM, together with the 95% confidence intervals of the regression analysis; values are given in Table 1, and the processes which act as sources or sinks for the 100 m carbon inventory are schematically summarized in Figure 3c.

[27] Vertical advection anomalies increase the surface DIC inventory by 3.6 ± 1.9 Pg C yr^{-1} per unit increase in the standardized SAM index south of 55°S. North of 55°S, vertical advection anomalies tend to decrease the surface DIC inventory by 3.4 ± 2.5 Pg C yr^{-1} (Table 1) so that an almost equal amount of carbon is transported into the surface layer in the south and exported to deeper layers in the north. This observation could not be made without quantifying the carbon transport directly [LM07, Lov07, *Le Quéré et al.*, 2007]. The DIC flux anomalies by horizontal advection nearly balance the vertical advection anomalies (Figure 3a). The northward DIC transport across any latitude is identical to the integral over J_{adv-h} between the southern model boundary and the latitude; it is maximal where the divergence J_{adv-h} passes through zero, near 55°S. Here a transport of 3.6 ± 1.2 Pg C yr^{-1} occurs, suggesting that stronger Ekman transport links upwelling and entrainment of carbon-rich water in the south (Ekman suction) and downwelling (Ekman pumping) in the north.

[28] The increase of DIC in the upper layer (Figure 1) is the result of these fluxes, which do not balance to zero; the DIC increase affects the pCO_2 gradient between ocean and atmosphere. D13 also found an increase in lateral advection but did not analyze the redistribution of carbon within the mixed layer that we find to be important for the latitudinal structure of the carbon budget.

[29] South of approximately 55°S, changes in upwelling tend to increase DIC but are largely offset by stronger northward advection, increased carbon export, and outgassing of CO_2. Interestingly, the increase in carbon export, which is attributable to diatoms, has a larger effect (additional export of 0.08 ± 0.04 Pg C yr^{-1}) than the outgassing of CO_2 (0.04 ± 0.02 Pg C yr^{-1}; Figure 3b). In contrast, export production north of the PF is reduced by 0.03 ± 0.05 Pg C yr^{-1}, and the carbon inventory increases in the surface layer; carbon is released to the atmosphere by stronger natural outgassing (0.09 ± 0.03 Pg C yr^{-1}, Table 1, Figure 3).

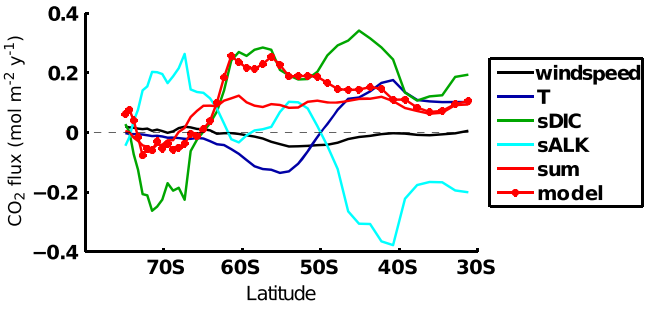

Figure 4. The effects of wind speed, temperature, salinity normalised DIC and alkalinity on the CO_2 flux at positive SAM (positive = outgassing). Note that the sum of the effects (red line) is smaller than the modelled (red dots) total response due to non-linearities.

We find that biological activity plays an important role for the SAM-induced interannual variability of carbon fluxes, in contrast to Lov07, and in agreement with *Wang and Moore* [2012]. The total effect of stronger natural carbon outgassing, integrated over the entire Southern Ocean (south of 30°S) amounts to 0.13 ± 0.05 Pg C yr^{-1} per unit standardized SAM index, which is within the uncertainty of previous studies (Lov07, LM07, D13).

3.3.2. Quantifying the Effect on CO_2 Fluxes

[30] The main drivers of CO_2 flux response to the SAM were identified following the equations given in Lov07 based on the linearized dependency of the sea-air CO_2 flux on changes of salinity-normalized DIC, salinity-normalized ALK, temperature, and wind fields as obtained by a regression onto the SAM index (Figure 4). Effects of sea ice, salinity, and freshwater flux changes on surface DIC and ALK had negligible contributions to CO_2 flux anomalies. The additional DIC source from intensified vertical advection is the main driver for the enhanced outgassing of natural carbon. Its effect on CO_2 fluxes is partly compensated by the effect of alkalinity as the additional vertical upward transport of DIC in the south and the downward transport in the north are accompanied by an anomalous ALK transport of the same magnitude (Figure 2) as first reported by D13. We find that the effects of additional DIC and alkalinity input do not balance each other in their effect on CO_2 fluxes (Figure 4), even though the input of DIC and alkalinity into the upper ocean are of the same magnitude with matching spatial distribution patterns (Figure 2). This agrees with the results of D13 and is explained by the nonlinearity of the carbonate system (D13).

[31] We find cooling south of 50°S and warming north of 50°S that agree with the general latitudinal structure for positive SAM phases derived from satellite observations [*Thompson et al.*, 2011]. Lov07 found a cooling effect throughout all latitudes and a maximum negative contribution to sea-air CO_2 flux anomalies of circa –0.2 mol m^{-2} yr^{-1}. Our maximum response is smaller with about –0.1 mol m^{-2} yr^{-1} but about 5–10 times larger than the temperature effect found in D13, who underestimated the temperature effect by only perturbing wind fields and not atmospheric temperature (D13).

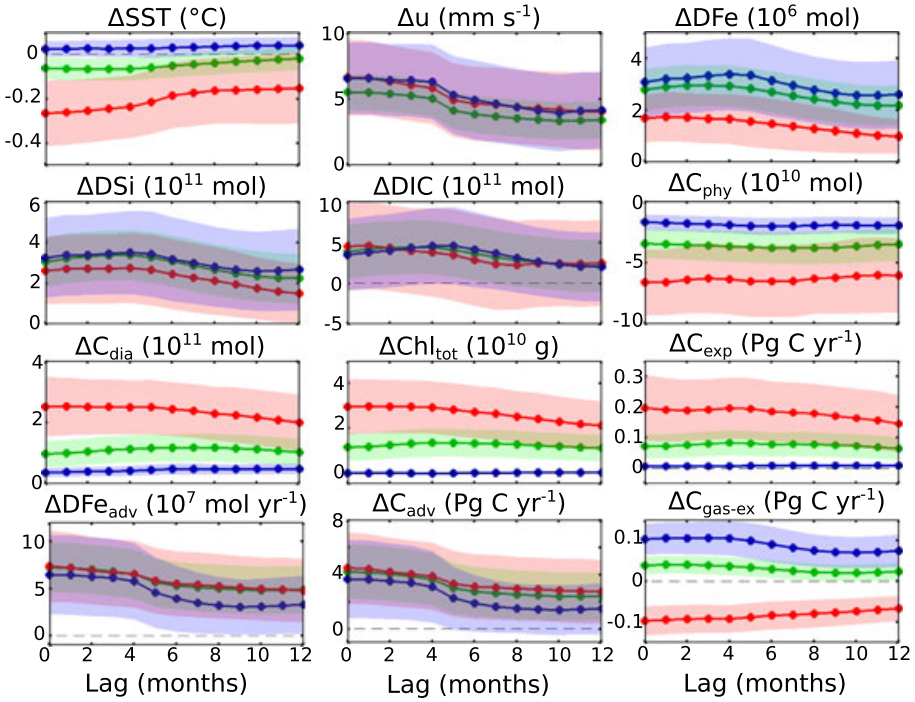

Figure 5. The response of (as indicated in the figures) average SST, zonal velocity (u), and inventories in the 0–10 m layer of DFe, DSi, DIC, nanophytoplankton carbon biomass (C_{phy}), diatom carbon biomass (C_{dia}), total chlorophyll (Chl_{tot}), and the anomalous fluxes at 100 m for export production (C_{exp}), DFe (DFe_{adv}), DIC (C_{adv}), and CO_2 flux at the surface ($C_{gas\text{-}ex}$) plotted versus lags 0 to 12 months. Shown are the annual mean response (green), summer (red), and winter (blue) and the 95% confidence intervals of the regression south of 55°S.

[32] We find a latitudinal structure with the largest contribution of DIC to natural CO_2 outgassing at 60°S and at 45°S (Figure 4) that differs from Lov07 and D13. As both studies only present averages within the Antarctic zone, polar frontal zone, subantarctic zone, and the subtropical zone, a direct comparison is not possible. We argue that it is more straightforward to report the full response versus latitude (Figure 4) because the position of the fronts depends, amongst other factors, on the resolution and will not be directly comparable to D13. Furthermore, two competing effects in our model would be averaged out in an integral over the Antarctic zone: DIC anomalies contribute to some CO_2 uptake along the coast, but they are balanced by an alkalinity effect of the same magnitude, and further north, the DIC effect peaks around 60°S.

[33] The degree of realism of the different modeling studies or the degree of difference between them is not the subject of this paper, but we would like to note that our experiment is different from that by D13 in several aspects. One major difference is that we analyze the mean response from 60 years of interannual varying forcing, while D13 analyzes 10 years of a system in quasiequilibrium with a constant wind perturbation superimposed on an otherwise unaltered, interannually varying atmospheric forcing. In addition, the analysis of linearized dependency of the sea-air CO_2 flux on DIC, ALK, wind, and temperature perturbations assumes that the system reacts approximately linearly. Indeed, the model's response shows the same structure as the sum of the individual responses, but the magnitude may differ so that the results of the analysis need to be interpreted with caution.

4. Timing and Seasonality

[34] The different responses between summer, winter, and the annual mean with lags of 0 to 12 months are presented in Figure 5. The largest response of surface current velocity and advection of carbon and nutrients across 100 m occurs immediately. The strong response persists until it lags the high-index polarity of the SAM by 4 months and has the same magnitude throughout all seasons. The sea surface temperature response is also largest at lag zero and decreases thereafter, but it is markedly different between seasons. The response of the SST to the SAM is strongest in summer, in line with previous studies [e.g., *Lovenduski and Gruber*, 2005; *Thompson et al.*, 2011].

[35] The maximum increase in the surface (top 10 m) concentration of DIC and nutrients lags the maximal vertical advection anomalies by about 4 months. As there is stronger upward transport of carbon and nutrients into the surface layer between 0 and 4 months lag, the surface layer keeps accumulating carbon and nutrients until the advection anomaly starts to become smaller. The responses of DSi, DFe, and DIC are very similar with two exceptions: (i) The maximum responses of surface DIC and DFe are largest at lag 4 to 5 in the annual mean and winter response but largest at a lag of zero in summer, indicating that carbon and nutrients are drawn down quickly by biological production. The difference in the magnitude of the response between the different lags, however, is small compared to the uncertainty of the regression. (ii) DSi and DFe show a weaker response in summer. In winter, nutrients can accumulate as photosynthesis is limited by light, whereas they can be immediately used in summer.

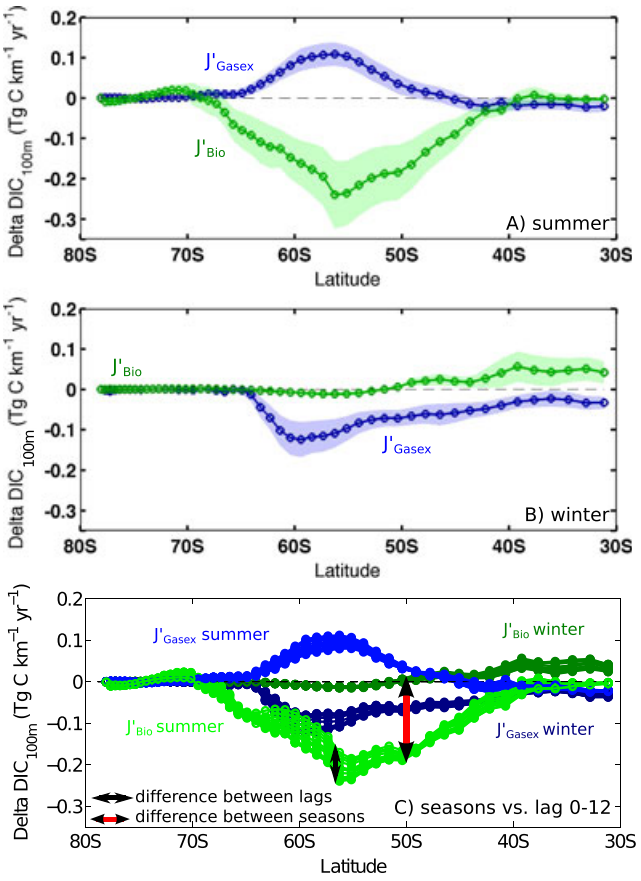

Figure 6. Same as Figure 3b but for (a) summer and (b) winter. (c) Zonally integrated summer and winter SAM effects of gas exchange and export production on the 100 m DIC inventory, plotted simultaneously (no confidence intervals for clarity), illustrating the small differences between lags as compared to huge differences between seasons.

[36] In the annual mean, the maximum response of phytoplankton biomass, chlorophyll, and export production is at 6 to 7 months, whereas it is at lag zero in summer. Both maxima follow the respective maxima in the surface iron concentration.

[37] Export production hardly changes during winter, and this is the season when outgassing of natural carbon occurs (Figures 5 and 6). In summer, on the contrary, export production is enhanced by additional nutrient availability, and this leads to an additional CO_2 uptake. Hence, the response of the CO_2 flux to the SAM index depends strongly on the season.

[38] The seasonal differences for latitudinally resolved export production and gas exchange are illustrated in Figure 6. In summer, export production increases and represents a carbon sink. This is directly reflected in an additional CO_2 uptake from the atmosphere which is, however, smaller in magnitude than the drawdown of carbon by export production. In winter, there is basically no change in export production in response to the positive SAM. As a result, the surface layer equilibrates with the atmospheric CO_2 content by releasing CO_2 into the atmosphere between 65°S and 30°S. The variability of response due to different lag times is

very small compared to the contrasting responses in different seasons (Figure 6c). Further studies are required to investigate whether this has implications on the carbon flux under a possible change of the seasonal distribution of the positive SAM trend [*Thompson et al.*, 2011].

[39] It was shown that in the annual mean response, CO_2 is released into the atmosphere; future change in the Southern Ocean carbon budget, however, depends on the balance between the SAM-mediated effects that enhance upwelling and mixing and direct climate change effects that may lead to warming and more stratification, i.e., less mixing. The trend toward the high-index polarity of the SAM is strongest in summer [*Thompson et al.*, 2011] so that it is possible that future climate change effects dominate in winter, and the SAM effect dominates in summer. In such a scenario, the SAM can be seen as natural iron fertilization that leads to additional uptake of natural carbon.

5. Concluding Remarks

[40] With a coupled ocean and ecosystem model, we can identify important, previously overlooked processes that determine the carbon budget during a positive SAM event also on seasonal timescales. These processes are (i) downward advective carbon fluxes north of the polar front (PF) as big as the upwelling fluxes in the south and (ii) export production that turns out to be a larger sink for natural carbon than CO_2 loss to the atmosphere by outgassing south of the PF in the annual mean.

[41] We show that the biological carbon pump plays an important role in the response to the SAM. This supports the correlation between CO_2 fluxes and export production that was previously suggested for decadal time scales by *Wang and Moore* [2012]. As the drawdown of carbon by primary production only occurs in summer and leads to less natural CO_2 outgassing (or more uptake) in that season, the future seasonal trend of the SAM index and the interaction with a global warming signal will determine the future of the Southern Ocean CO_2 sink.

[42] *Lenton et al.* [2009] hypothesized that iron supply during a positive SAM phase induces changes in the C:Chl ratio to explain the increase in chlorophyll [*Lovenduski and Gruber*, 2005] and argued for a weak response by primary production. In contrast, we show that both carbon and chlorophyll increase during positive SAM periods by taking into account acclimation of cellular stoichiometry (N:C:Chl:Si for diatoms and N:C:Chl for non-diatoms) to light and nutrient conditions.

[43] Our analysis does not resolve which physical mechanism (isopycnal and diapycnal mixing, advection) ultimately transports the carbon advected from below into the mixed layer, as opposed to over the 100 m depth level. Further, all results were obtained with a model that parameterizes eddies so that important eddy compensation effects [*Böning et al.*, 2008] are not investigated. The response of eddies, however, is delayed by 2 to 3 years [*Meredith and Hogg*, 2006; *Screen et al.*, 2009], whereas the SAM oscillates between its high and low polarity on time scales of weeks to months [*Thompson et al.*, 2011] so that the system never equilibrates on the time scale that we consider. It remains questionable whether full eddy compensation can develop on that time scale. In a first eddy-permitting study, D13 calculated a very similar quantity of additional outgassing of natural CO_2 during positive SAM periods (0.1 Pg C yr^{-1}) as we do. While D13's results support ours, they assumed that the system is equilibrated with stronger winds at a positive SAM and is therefore focused on the long-term trend predicted for the future rather than on interannual variability so that further comparative studies are required for more definite conclusions.

[44] Studies of the response of Southern Ocean carbon fluxes to the SAM use a variety of physical and biogeochemical models, model resolutions, experimental designs, and methods to analyze the results [Lov07, LM07, D13, *Le Quéré et al.*, 2007]. All come to the result that the contemporary carbon sink is reduced by about 0.1 Pg C yr^{-1} per unit of standardized SAM index, implying that this is a robust result, but each of the studies addresses slightly different questions (interannual variability versus long-term equilibrium) and uses different approaches for the analysis. No previous study reported seasonal differences. A detailed model and method comparison study would be valuable to further the understanding of the seasonal differences and to shed light on the mechanisms that lead to different latitudinal structures.

[45] **Acknowledgments.** We thank Natalie Mahowald for providing dust fields. This research was supported through EU FP7 project CARBOCHANGE (grant agreement 264879) and through the German project BIOACID, funded by the Federal Ministry of Education and Research (BMBF, FKZ 03F0608B).

References

Aumont, O., J. C. Orr, P. Monfray, G. Madec, and E. Maier-Reimer (1999), Nutrient trapping in the equatorial Pacific: The ocean circulation solution, *Global Biogeochem. Cycles*, *13*, 351–369, doi:10.1029/1998GB900012.

Böning, C. W., A. Dispert, M. Visbeck, S. R. Rintoul, and F. U. Schwarzkopf (2008), The response of the Antarctic Circumpolar Current to recent climate change, *Nat. Geosci.*, *1*, 864–869, doi:10.1038/ngeo362.

Campin, J.-M., and H. Goosse (1999), Parameterization of density-driven downsloping flow for a coarse-resolution ocean model in z-coordinate, *Tellus A*, *51*, 412–430, doi:10.1034/j.1600-0870.1999.t01-3-00006.x.

de Baar, H. J. W., L. J. A. Gerringa, P. Laan, and K. R. Timmermans (2008), Efficiency of carbon removal per added iron in ocean iron fertilization, *Mar. Ecol. Prog. Ser.*, *364*, 269–282, doi:10.3354/meps07548.

Dufour, C. O., J. Le Sommer, J. D. Zika, M. Gehlen, J. C. Orr, P. Mathiot, and B. Barnier (2012), Standing and transient eddies in the response of the Southern Ocean meridional overturning to the southern annular mode, *J. Clim.*, *25*, 6958–6974.

Dufour, C. O., J. Le Sommer, M. Gehlen, J. C. Orr, J.-M. Molines, J. Simeon, and B. Barnier (2013), Eddy compensation and controls of the enhanced sea-to-air CO_2 flux during positive phases of the southern annular mode, *Global Biogeochem. Cycles*, *27*, 950–961, doi:10.1002/gbc.20090.

Geider, R. J., H. L. MacIntyre, and T. M. Kana (1998), A dynamic regulatory model of phytoplankton acclimation to light, nutrients, and temperature, *Limnol. Oceanogr.*, *43*, 679–694, doi:10.4319/lo.1998.43.4.0679.

Gent, P. R., and J. C. McWilliams (1990), Isopycnal mixing in ocean circulation models, *J. Phys. Oceanogr.*, *20*, 150–155.

Gentleman, W., A. Leising, B. Frost, S. Strom, and J. Murray (2003), Functional responses for zooplankton feeding on multiple resources: A review of assumptions and biological dynamics, *Deep Sea Res. Part II*, *50*, 2847–2875, doi:10.1016/j.dsr2.2003.07.001.

Hall, A., and M. Visbeck (2002), Synchronous variability in the Southern Hemisphere atmosphere, sea ice, and ocean resulting from the annular mode, *J. Clim.*, *15*, 3043–3057.

Hallberg, R., and A. Gnanadesikan (2006), The role of eddies in determining the structure and response of the wind-driven Southern Hemisphere overturning: Results from the modeling eddies in the Southern Ocean (MESO) project, *J. Phys. Oceanogr.*, *36*, 2232–2252, doi:10.1175/JPO2980.1.

Hogg, A. M., M. P. Meredith, J. R. Blundell, and C. Wilson (2008), Eddy heat flux in the Southern Ocean: Response to variable wind forcing, *J. Clim.*, *21*, 608–620, doi:10.1175/2007JCLI1925.1.

Hohn, S. (2009), Coupling and decoupling of biogeochemical cycles in marine ecosystems, PhD Thesis, Universität Bremen. http://elib.suub.uni-bremen.de/diss/docs/00011278pdf.

Hoppema, M. (2004), Weddell Sea turned from source to sink for atmospheric CO_2 between pre-industrial time and present, *Global Planet. Change*, *40*, 219–231, doi:10.1016/j.gloplacha.2003.08.001.

Kara, A. B., P. A. Rochford, and H. E. Hurlburt (2000), An optimal definition for ocean mixed layer depth, *J. Geophys. Res.*, *105*, 16,803–16,821, doi:10.1029/2000JC900072.

Khatiwala, S., F. Primeau, and T. Hall (2009), Reconstruction of the history of anthropogenic CO_2 concentrations in the ocean, *Nature*, *462*, 346–349, doi:10.1038/nature08526.

Kriest, I., and A. Oschlies (2008), On the treatment of particulate organic matter sinking in large-scale models of marine biogeochemical cycles, *Biogeosciences*, *5*, 55–72, doi:10.5194/bg-5-55-2008.

Large, W. G., G. Danabasoglu, S. C. Doney, and J. McWilliams (1997), Sensitivity to surface forcing and boundary layer mixing in a global ocean model: Annual-mean climatology, *J. Phys. Oceanogr.*, *27*, 2418–2447.

Law, R. M., R. J. Matear, and R. J. Francey (2008), Comment on: "Saturation of the Southern Ocean CO_2 sink due to recent climate change", *Science*, *319*, 570a, doi:10.1126/science.1149077.

Le Quéré, C., et al. (2007), Saturation of the Southern Ocean CO_2 sink due to recent climate change, *Science*, *316*, 1735–1738, doi:10.1126/science.1136188.

Le Quéré, C., et al. (2008), Response to Comments on "Saturation of the Southern Ocean CO_2 sink due to recent climate change, *Science*, *319*, 570c, doi:10.1126/science.1147315.

Lenton, A., and R. J. Matear (2007), Role of the southern annular mode (SAM) in Southern Ocean CO_2 uptake, *Global Biogeochem. Cycles*, *21*, GB2016, doi:10.1029/2006GB002714.

Lenton, A., F. Codron, L. Bopp, N. Metzl, P. Cadule, A. Tagliabue, and J. Le Sommer (2009), Stratospheric ozone depletion reduces ocean carbon uptake and enhances ocean acidification, *Geophys. Res. Lett.*, *36*, L12606, doi:10.1029/2009GL038227.

Losch, M., D. Menemenlis, J.-M. Campin, P. Heimbach, and C. Hill (2010), On the formulation of sea-ice models. Part 1: Effects of different solver implementations and parameterizations, *Ocean Modell.*, *33*, 129–144, doi:10.1016/j.ocemod.2009.12.008.

Lovenduski, N. S., and N. Gruber (2005), Impact of the southern annular mode on Southern Ocean circulation and biology, *Geophys. Res. Lett.*, *32*, L11603, doi:10.1029/2005GL022727.

Lovenduski, N. S., N. Gruber, S. C. Doney, and I. D. Lima (2007), Enhanced CO_2 outgassing in the Southern Ocean from a positive phase of the southern annular mode, *Global Biogeochem. Cycles*, *21*, GB2026, doi:10.1029/2006GB002900.

Lovenduski, N. S., N. Gruber, and S. C. Doney (2008), Toward a mechanistic understanding of the decadal trends in the Southern Ocean carbon sink, *Global Biogeochem. Cycles*, *22*, GB3016, doi:10.1029/2007GB003139.

Lovenduski, N. S., M. C. Long, P. R. Gent, and K. Lindsay (2013), Multi-decadal trends in the advection and mixing of natural carbon in the Southern Ocean, *Geophys. Res. Lett.*, *40*, 139–142, doi:10.1029/2012GL054483.

Marinov, I., A. Gnanadesikan, J. R. Toggweiler, and J. L. Sarmiento (2006), The Southern Ocean biogeochemical divide, *Nature*, *441*, 964–967, doi:10.1038/nature04883.

Marshall, G. J. (2003), Trends in the southern annular mode from observations and reanalyses, *J. Clim.*, *16*, 4134–4143.

Marshall, J., and K. Speer (2012), Closure of the meridional overturning circulation through Southern Ocean upwelling, *Nat. Geosci.*, *5*, 171–180, doi:10.1038/ngeo1391.

Marshall, J., A. Adcroft, C. Hill, L. Perelman, and C. Heisey (1997), A finite-volume, incompressible Navier Stokes model for studies of the ocean on parallel computers, *J. Geophys. Res.*, *102*, 5753–5766, doi:10.1029/96JC02775.

Matear, R. J., and A. Lenton (2008), Impact of historical climate change on the Southern Ocean carbon cycle, *J. Clim.*, *21*, 5820–5834, doi:10.1175/2008JCLI2194.1.

Meredith, M. P., A. C. Naveira Garabato, A. M. Hogg, and R. Farneti (2012), Sensitivity of the overturning circulation in the Southern Ocean to decadal changes in wind forcing, *J. Clim.*, *25*, 99–110, doi:10.1175/2011JCLI4204.1.

Meredith, P. M., and A. M. Hogg (2006), Circumpolar response of Southern Ocean eddy activity to a change in the southern annular mode, *Geophys. Res. Lett.*, *33*, L16608, doi:10.1029/2006GL026499.

Mikaloff Fletcher, S. E., et al. (2007), Inverse estimates of the oceanic sources and sinks of natural CO_2 and the implied oceanic carbon transport, *Global Biogeochem. Cycles*, *21*, GB1010, doi:10.1029/2006GB002751.

MITgcm Group (2012), *MITgcm User Manual (online documentation)*, MIT/EAPS, Cambridge, Mass., available at http://mitgcm.org/public/r2_manual/latest/online_documents/manual.html.

Moore, J. K., S. C. Doney, and K. Lindsay (2004), Upper ocean ecosystem dynamics and iron cycling in a global three-dimensional model, *Global Biogeochem. Cycles*, *18*, GB4028, doi:10.1029/2004GB002220.

Morrison, A. K., and A. M. Hogg (2013), On the relationship between Southern Ocean overturning and ACC transport, *J. Phys. Oceanogr.*, *43*, 140–148, doi:10.1175/JPO-D-12-057.1.

Orsi, A. H., T. Whitworth, and W. D. Nowlin (1995), On the meridional extent and fronts of the Antarctic Circumpolar Current, *Deep Sea Res. Part I Oceanogr. Res. Pap.*, *42*, 641–673, doi:10.1016/0967-0637(95)00021-W.

Sallée, J. B., K. G. Speer, and S. R. Rintoul (2010), Zonally asymmetric response of the Southern Ocean mixed-layer depth to the southern annular mode, *Nat. Geosci.*, *3*, 273–279, doi:10.1038/NGEO812.

Schartau, M., A. Engel, J. Schröter, S. Thoms, C. Völker, and D. Wolf-Gladrow (2007), Modelling carbon overconsumption and the formation of extracellular particulate organic carbon, *Biogeosciences*, *4*, 433–454, doi:10.5194/bg-4-433-2007.

Screen, J. A., N. P. Gillett, D. P. Stevens, G. J. Marshall, and H. K. Roscoe (2009), The role of eddies in the Southern Ocean temperature response to the southern annular mode, *J. Clim.*, *22*, 806–818, doi:10.1175/2008JCLI2416.1.

Sen Gupta, A., and M. H. England (2006), Coupled ocean-atmosphere-ice response to variations in the southern annular mode, *J. Clim.*, *19*, 4457–4486, doi:10.1175/JCLI3843.1.

Spence, P., J. C. Fyfe, A. Montenegro, and A. J. Weaver (2010), Southern Ocean response to strengthening winds in an eddy-permitting global climate model, *J. Clim.*, *23*, 5332–5343, doi:10.1175/2010JCLI3098.1.

Thompson, D. W. J., and J. M. Wallace (2000), Annular modes in the extratropical circulation. Part I: Month-to-month variability, *J. Clim.*, *13*, 1000–1016.

Thompson, D. W. J., S. Solomon, P. J. Kushner, M. H. England, K. M. Grise, and D. J. Karoly (2011), Signatures of the Antarctic ozone hole in Southern Hemisphere surface climate change, *Nat. Geosci.*, *4*, 741–749, doi:10.1038/ngeo1296.

Timmermann, R., et al. (2010), A consistent data set of Antarctic ice sheet topography, cavity geometry, and global bathymetry, *Earth Syst. Sci. Data*, *2*, 261–273, doi:10.5194/essd-2-261-2010.

Wang, S., and J. K. Moore (2012), Variability of primary production and air-sea CO_2 flux in the Southern Ocean, *Global Biogeochem. Cycles*, *26*, GB1008, doi:10.1029/2010GB003981.

Wanninkhof, R. (1992), Relationship between wind speed and gas exchange over the ocean, *J. Geophys. Res.*, *97*, 7373–7382, doi:10.1029/92JC00188.

Zickfeld, K., J. C. Fyfe, M. Eby, and A. J. Weaver (2008), Comment on "Saturation of the Southern Ocean CO_2 sink due to recent climate change," *Science*, *319*, 570b, doi:10.1126/science.1146886.